Molecular Therapy
Nucleic Acids
Original Article

Lipid self-assembling nanoparticles as a novel platform for mRNA-based vaccination

Arianna De Chiara,[1,2,10] Valeria Nele,[3,10] Alessia Angelillo,[3] Virginia Campani,[4] Andrea Campanile,[1,2] Guendalina Froechlich,[1,2] Annagiulia Scognamiglio,[1,2] Emilio Pellino,[1,2] Antonietta Greco,[5] Clizia Chinello,[6] Lisa Pagani,[6] Remo Eugster,[7] Paola Luciani,[7] Claudia Corbo,[5,8] Alfredo Nicosia,[1,2,9,11] Emanuele Sasso,[1,2,9,11] and Giuseppe De Rosa[3,11]

[1]CEINGE—Biotecnologie Avanzate S.c.a.r.l., Via Gaetano Salvatore 486, 80131 Naples, Italy; [2]Department of Molecular Medicine and Medical Biotechnology, University of Naples Federico II, Via Pansini 5, 80131 Naples, Italy; [3]Department of Pharmacy, University of Naples Federico II, Via D. Montesano 49, 80131 Naples, Italy; [4]Department of Life Health Sciences and Health Profession, Link Campus University, Via del Casale di S. Pio V 44, 00165 Rome, Italy; [5]NANOMIB Center, Department of Medicine and Surgery, University of Milano-Bicocca, Via Raoul Follereau 3, 20854 Vedano al Lambro, Italy; [6]Proteomics and Metabolomics Unit, Department of Medicine and Surgery, University of Milano-Bicocca, Via Raoul Follereau 3, 20854 Vedano al Lambro, Italy; [7]Department of Chemistry, Biochemistry and Pharmaceutical Sciences, University of Bern, Freiestrasse 3, 3012 Bern, Switzerland; [8]IRCCS Istituto Ortopedico Galeazzi, Via Cristina Belgioioso 173, 20161 Milan, Italy; [9]ImGen-T Srl, Viale del Parco Carelli 70, 80123 Naples, Italy

Synthetic messenger RNA (mRNA) formulated in lipid nanoparticles (mRNA-LNPs) is a promising candidate for next-generation gene therapy and genetic vaccines. However, mRNA-LNP formulations require low-temperature storage to ensure proper transport and distribution. Here, we introduce a lipid self-assembling nanoparticle (SANP) technology to address the stability challenges of mRNA-based therapeutics. SANP formulations can be prepared by simply mixing the components immediately before use, allowing mRNA vaccines to be stored and transported at 4°C without freezing, thereby enhancing their stability. SANPs loaded with mRNA (mRNA-SANPs) exhibited a sub-200 nm size, high mRNA encapsulation efficiency, colloidal stability post-assembly and in human plasma, and low hemolytic activity. Intramuscular (IM) and intravenous (IV) administration of mRNA-SANPs encoding a reporter gene in mice resulted in high levels of transgene expression, with no observed renal or hepatic toxicity and no release of pro-inflammatory cytokines. Additionally, protein fingerprint analysis of mRNA-SANPs in serum identified specific nanoparticle-protein interactions that correlated with *in vivo* biodistribution. Finally, mRNA-SANPs encoding the severe acute respiratory syndrome coronavirus 2 (SARS-CoV-2) spike protein elicited a significant immune response in mice following both IM and IV administration.

INTRODUCTION

The recent severe acute respiratory syndrome coronavirus 2 (SARS-CoV-2) pandemic outbreak has led to the development of highly efficacious genetic vaccines based on synthetic messenger RNA (mRNA) encoding the full-length spike protein of the SARS-CoV-2 virus (Gene ID: 1489668).[1,2] mRNA-based vaccines offer several advantages over conventional vaccine platforms: they can be rapidly designed and produced at large scale, are not associated with the risk of infection or insertional mutagenesis,[3] and can be re-administered multiple times. Furthermore, the mRNA sequence can be designed to ensure the production of complex antigens, such as transmembrane or multimeric proteins, and it is possible to use mRNAs encoding different antigens within a single formulation.[4] These features make mRNA technology highly attractive for the development of prophylactic vaccines against infectious diseases and cancer.[4,5] Beyond genetic vaccines, mRNA is also emerging as a valuable tool for gene replacement therapies and genome editing applications (e.g., Cas9).[6]

However, mRNA is highly susceptible to nuclease-mediated degradation, both *in vitro* and *in vivo*, and cannot cross the cell membrane, thus requiring nanocarriers for protection and cellular delivery.[7] Several non-viral nanocarriers have been proposed, among which lipid nanoparticles (LNPs) represent the most successful example, particularly following the approval of two LNP-formulated SARS-CoV-2 mRNA vaccines[1,2]). Despite their success, mRNA-LNPs exhibit limited stability at temperatures $\geq 4°C$ and require storage and transport at temperatures below $-20°C$,[8,9] significantly

Received 7 May 2025; accepted 28 January 2026;
https://doi.org/10.1016/j.omtn.2026.102851.

[10]These authors contributed equally

[11]These authors contributed equally

Correspondence: Alfredo Nicosia, CEINGE—Biotecnologie Avanzate S.c.a.r.l., Via Gaetano Salvatore 486, 80131 Naples, Italy.
E-mail: alfredo.nicosia@unina.it
Correspondence: Emanuele Sasso, CEINGE—Biotecnologie Avanzate S.c.a.r.l., Via Gaetano Salvatore 486, 80131 Naples, Italy.
E-mail: emanuele.sasso@unina.it
Correspondence: Giuseppe De Rosa, Department of Pharmacy, University of Naples Federico II, Via D. Montesano 49, 80131 Naples, Italy.
E-mail: gderosa@unina.it

increasing cold-chain costs and the risk of vaccine spoilage and mishandling by non-experienced users. To overcome this issue, alternative strategies are being explored, including the lyophilization of mRNA-LNPs,[10] the spray-drying of small interfering RNA (siRNA)-LNPs,[11,12] and the design of formulations with enhanced thermal stability.[13]

A promising strategy to circumvent the stability limitations of mRNA formulations involves loading the mRNA into the nanocarrier immediately before administration. Lipoplexes, which are obtained by mixing cationic liposomes with mRNA in defined ratios, are an example of this approach. While originally devised as *in vitro* transfection agents,[14] lipoplexes are currently under investigation in several clinical trials as anti-cancer mRNA vaccines.[15] Core-shell lipid-based nanoparticles (NPs) can also be proposed as an alternative platform for *in vivo* mRNA delivery. These nanoparticles typically comprise a core material, which encapsulates the payload, and a lipid shell. Core materials include polypeptides, hyaluronic acid, chitosan, calcium phosphate (CaP), and synthetic polymers.[16] Among these, CaP cores are particularly appealing due to ease of synthesis, low cytotoxicity, strong electrostatic interaction with negatively charged molecules (i.e., nucleic acids), and pH responsiveness, which enables payload release following dissolution of the CaP core in the acidic environment of cellular endosomes.[17]

We previously developed hybrid lipid self-assembling nanoparticles (SANPs) with a CaP core for the encapsulation of bisphosphonates, which have been successfully tested *in vivo* for the treatment of prostate cancer[18,19] and glioblastoma.[20] This formulation has also received the Orphan Drug Designation from the European Medicines Agency (EMA) and Food and Drug Administration (FDA) (29/08/2016-EU/3/16/1735) for the treatment of high-grade glioma, which supports its potential for broader clinical applications. More recently, we have demonstrated the ability of SANPs to deliver microRNA (miRNA)[21] and siRNA[22] to the mouse brain for the treatment of glioblastoma. SANP formulations exhibit several advantages, such as good biocompatibility, high efficiency of RNA encapsulation, and intracellular delivery. Importantly, the SANP technology is based on the *in situ* mixing of its components (i.e., CaP NPs, cationic liposomes, and mRNA) immediately prior to use. This modular approach enables storage and transport of the mRNA in lyophilized form, which ensures improved stability against degradation compared to freezing. As such, lipid SANPs may represent a viable platform for the formulation of next-generation synthetic mRNA-based therapeutics.

To evaluate the feasibility of the SANP technology for the *in vivo* delivery of large synthetic *in vitro* transcribed (IVT) mRNA, we developed SANP formulations encapsulating mRNA upon component mixing at room temperature. These formulations were comprehensively characterized for their physicochemical properties, mRNA encapsulation efficiency, colloidal stability, stability against aggregation in human plasma, hemolytic activity, and *in vitro* transfection ability. We then assessed both organ-specific and systemic inflammatory responses following mRNA-SANP administration in mice. The expression kinetics of mRNA encoding reporter genes were evaluated following intravenous (IV) or intramuscular (IM) injection. To gain further insights into the *in vivo* behavior of mRNA-SANPs, we characterized the SANP protein corona (PC) composition and correlated these findings with *in vivo* biodistribution data. Finally, we demonstrated that mRNA-SANP formulations encoding the SARS-CoV-2 spike protein could elicit potent T cell responses, as well as significant humoral immunity, in mice.

RESULTS

Development and characterization of mRNA-SANP formulations

The formulation of SANPs requires the use of cationic lipids able to interact with the CaP core encapsulating the anionic mRNA. Here, we chose 1,2-dioleoyl-3-trimethylammonium-propane chloride (DOTAP) as the cationic lipid for SANP formulations; this lipid has been extensively investigated for the formulation of cationic LNPs. Its chemical structure comprises two unsaturated alkyl chains connected to a trimethylammonium-propane head group *via* hydrolyzable ester bonds, which make this lipid biodegradable. DOTAP-based SANP formulations outperformed those based on other cationic lipids in terms of stability against aggregation in human plasma, hemolytic activity, and intracellular miRNA uptake in glioblastoma cells.[21] Furthermore, DOTAP-containing liposomes have been shown to have an immunostimulatory effect on dendritic cells, both *in vitro* and *in vivo*, which may be advantageous for genetic vaccine applications.[23,24] To enhance nanoparticle stability against aggregation in complex biological fluids, such as serum, we enriched the SANP formulation with a PEGylated lipid, i.e., N-palmitoyl-sphingosine-1-{succinyl[methoxy(polyethylene glycol)2000]}($Cer_{16}PEG_{2000}$).

mRNA-loaded SANPs (mRNA-SANPs) were assembled by mixing the mRNA solution, the CaP NPs, and the cationic liposomes in appropriate ratios (Figure 1A). Here, we prepared mRNA-loaded SANPs with an N/P = 9 and a final mRNA concentration of 200 μg/mL. To explore the flexibility of this approach and investigate the influence of mRNA length on the colloidal characteristics of SANP formulations, we used two clinically relevant mRNA constructs of different lengths: one encoding the full-length coronavirus disease 2019 (COVID-19) spike protein (spike; 4,150 nucleotides long) and one encoding the receptor-binding domain (RBD) of the spike protein (1,047 nucleotides long). The two mRNAs were synthesized by T7-mediated *in vitro* transcription using CAP1 and N1-methyl-pseudouridine triphosphate and included a segmented 100-nucleotide-long poly(A) tail. Following *in vitro* transcription, the integrity and identity of the mRNA were confirmed by capillary electrophoresis (Figure S1).

We used dynamic light scattering (DLS) to determine the z-average diameter, polydispersity index (PDI), and zeta potential of the mRNA-SANPs, while the mRNA encapsulation efficiency was measured by the RiboGreen assay. We observed minimal changes

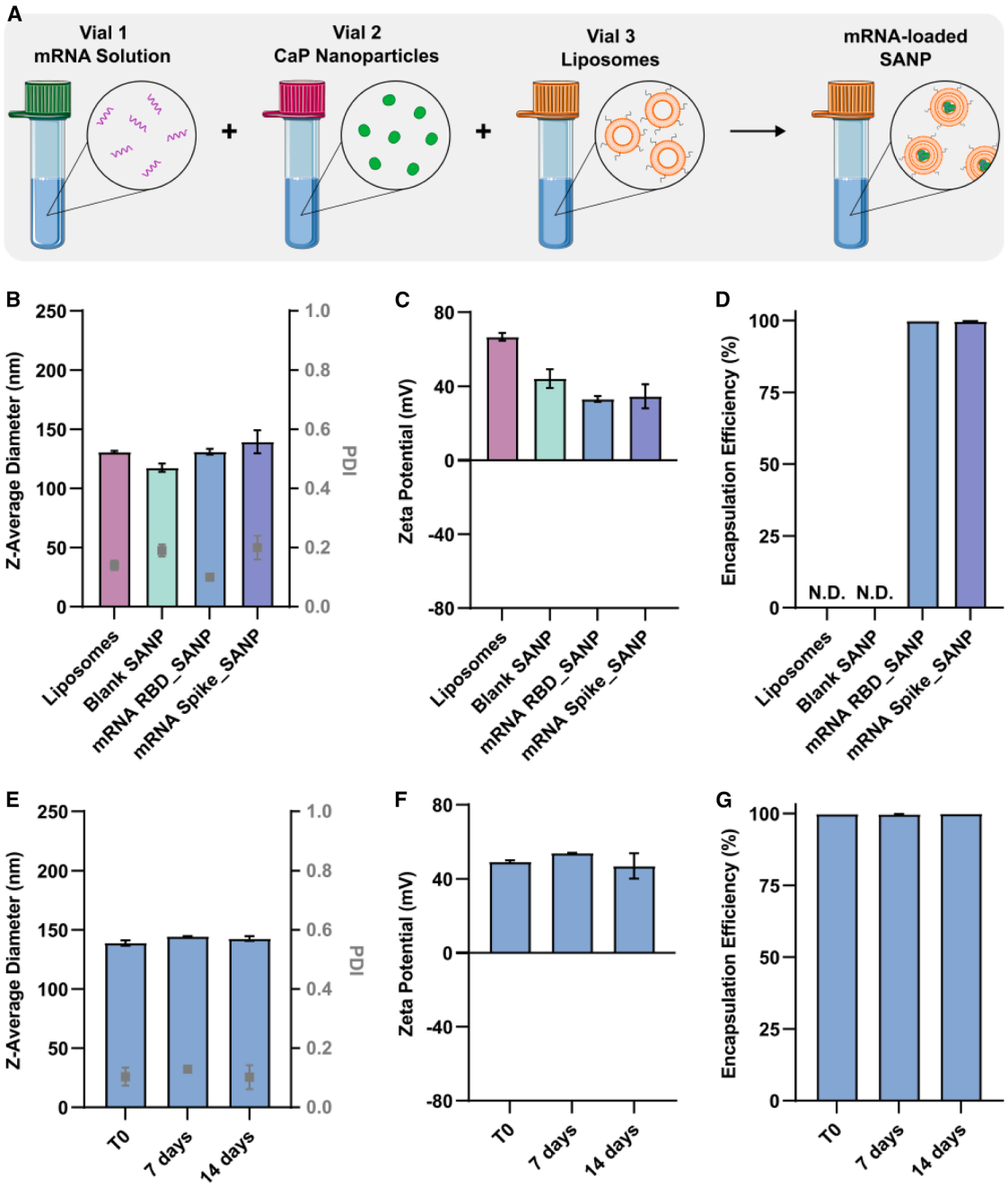

Figure 1. Physicochemical properties of mRNA-SANPs

(A) Assembly of mRNA-loaded SANP formulations, achieved by mixing mRNA, CaP NPs, and cationic liposomes. Part of the schematic was created with Servier Medical Art. Z-average diameter and PDI (B), zeta potential (C), and mRNA encapsulation efficiency (D) were measured for cationic liposomes, blank SANPs, and SANPs encapsulating mRNA encoding either the RBD or the spike protein. The colloidal stability of SANP formulations encapsulating mRNA encoding GFP was measured up to 14 days post-assembly at 4 °C in terms of z-average diameter and PDI (E), zeta potential (F), and mRNA encapsulation efficiency (G). The final concentration of formulated mRNA was 200 μg/mL, with an N/P = 9. Data are shown as mean ± SD of *N* = 3 independent batches.

in z-average diameter and PDI of mRNA-loaded SANPs compared to liposomes and blank SANPs, regardless of the mRNA length (Figure 1B). We detected a reduction in the zeta potential for SANP formulations compared to the starting liposomes, suggesting lipid reorganization during assembly and the presence of mRNA molecules on the SANP surface (Figure 1C). The mRNA

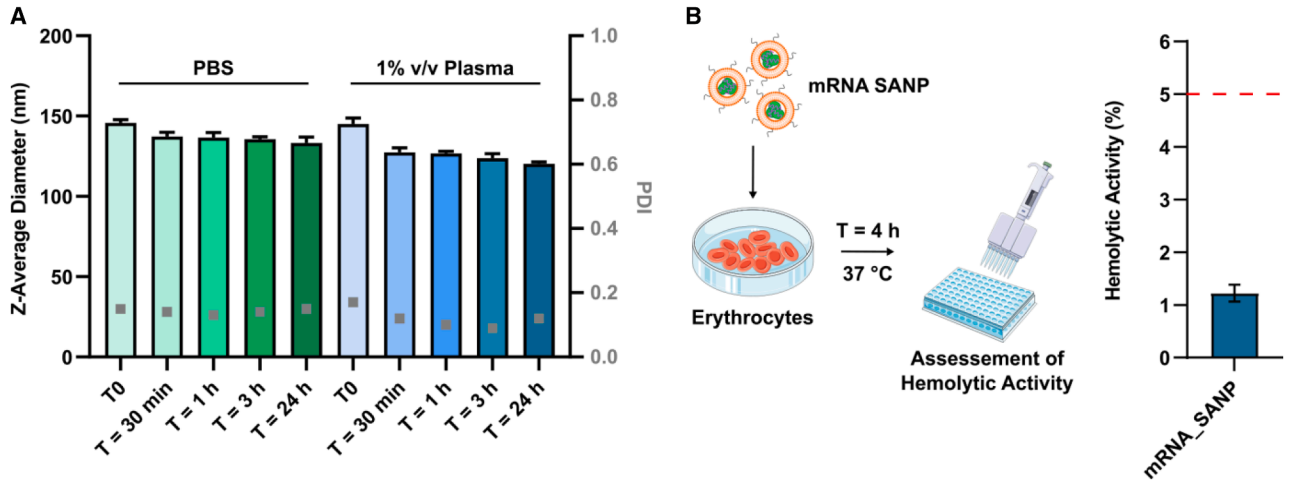

Figure 2. Colloidal and hemolytic properties of mRNA-SANPs

(A) Colloidal stability of mRNA-SANPs diluted to 20 μg/mL in either PBS or 1% v/v human plasma. The formulations were incubated at 37 °C, and the mean hydrodynamic diameter was measured immediately after dilution, as well as at 30 min, 1, 3, and 24 h post-dilution. Measurements were carried out in triplicate. (B) Schematic of the hemolysis assay and hemolytic activity of mRNA-SANP formulations. Part of the schematic was created with Servier Medical Art. Data are shown as mean ± SD of $N = 3$ independent experiments, with $n \geq 2$ technical replicates.

encapsulation efficiency was higher than 98% for both mRNA molecules, whose length did not affect the colloidal properties of the final nanoparticles (Figure 1D). Preliminary cryogenic transmission electron microscopy (cryo-TEM) experiments (Figure S2) revealed that SANPs encapsulating mRNA exhibit a double bilayer structure, in analogy to what has been previously observed for SANPs loaded with zoledronic acid.[25] More complex, multilayered structures were also present in the sample. Despite SANP being a technology designed for extemporaneous preparation in a hospital pharmacy, future studies will be needed to determine the complexation efficiency of the CaP NPs and the cationic liposomes in the presence of mRNA for quality assessment of the formulations prior to clinical studies. Small-angle neutron and X-ray scattering studies will be carried out in the future to precisely unravel the structure of the mRNA-SANP formulations.

To gain insights into the colloidal stability of mRNA-SANP formulations upon storage at 4°C, we probed the z-average diameter, PDI, zeta potential, and mRNA encapsulation efficiency at 7 and 14 days post-assembly. We observed minimal changes in size, surface charge, and mRNA encapsulation efficiency of mRNA-SANPs over this time frame (Figures 1E–1G), suggesting that mRNA-SANPs can also be assembled and stored at 4 °C for up to 14 days without compromising their physicochemical features.

As previously stated, the main aim of this study was to investigate the ability of SANP formulations to deliver large synthetic mRNAs into the cytoplasm of eukaryotic cells to allow translation. We therefore assessed the ability of SANPs to transduce a reporter gene mRNA (i.e., mRNA encoding enhanced green fluorescent protein [eGFP]) *in vitro* in 80% confluent HeLa cells, either immediately after formulation (T0) or after 7 and 14 days of storage at 4°C (Figure S3). Lipofectamine 3000 was used as a positive control for the assay. Twenty-four hours post-transfection, cells were detached and analyzed for fluorescence by flow cytometry. Both Lipofectamine 3000 and SANP formulations showed a similar percentage of eGFP-positive cells at T0. To further evaluate the stability of SANPs, freshly seeded HeLa cells were transfected with SANPs stored for 7 and 14 days at 4°C; flow cytometry analysis revealed that SANP activity at 7 days remained relatively stable compared to as-prepared formulations (74% vs. 65% eGFP-positive cells). However, although the percentage of eGFP-positive cells remained relatively high (∼60%), SANP activity was significantly compromised after 14 days of storage at 4°C (Figure S3).

As a preliminary evaluation of the suitability of mRNA-SANPs for *in vivo* administration, we assessed the colloidal stability of mRNA-SANPs against aggregation in the presence of human plasma. The formulations were diluted in 1% v/v human plasma or phosphate-buffered saline (PBS) as a control, and their mean hydrodynamic diameter was determined immediately after dilution, as well as 30 min, 1, 3, and 24 h post-dilution at 37°C. Minimal changes in the hydrodynamic diameter of mRNA-SANPs were detected over the investigated time frame in human plasma, suggesting that the formulations are colloidally stable under these conditions (Figure 2A). In this work, a preliminary stability assessment was carried out in 1% v/v human plasma; future studies of the physicochemical stability of mRNA-SANP formulations in 50% v/v or full plasma will provide additional insights into the behavior of the nanoparticles in biologically relevant environments.

When designing nanoparticle formulations for intravenous administration, it is crucial to assess their hemolytic properties. The hemolysis assay established by the American Society for Testing and

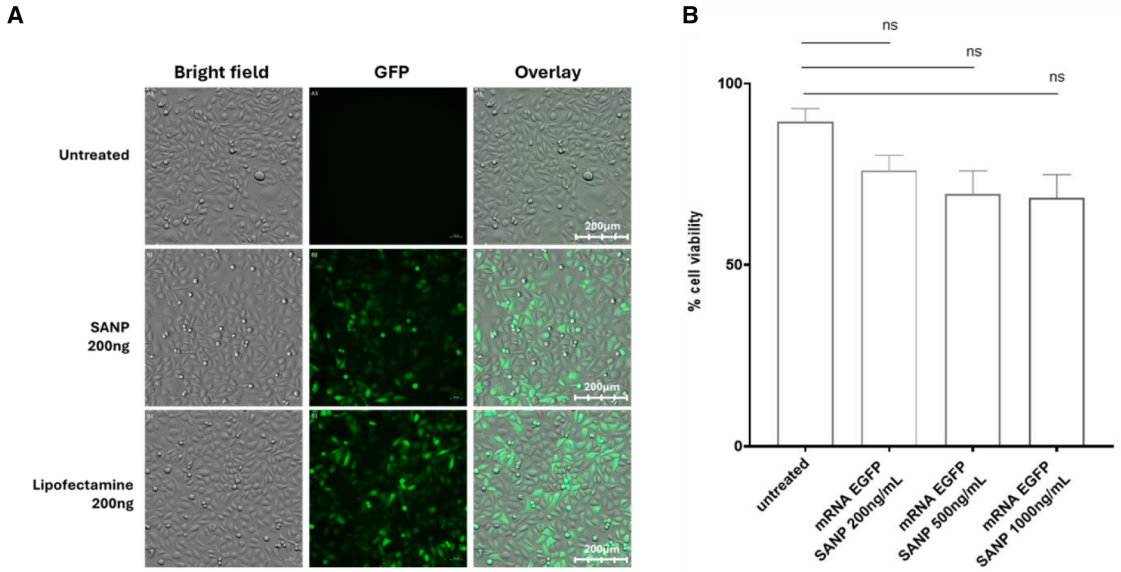

Figure 3. *In vitro* biological effects of mRNA-SANPs

(A) Transfection efficiency of eGFP mRNA formulated with SANPs or Lipofectamine 3000. Monolayers of HeLa cells were transfected with either 200 ng/mL of mRNA eGFP-SANPs or 200 ng/mL of eGFP-Lipofectamine 3000. Cells were analyzed by fluorescent microscopy 24 h post-transfection. Mock-transfected cells were used as a negative control (untreated). (B) Cell viability upon incubation with varying concentrations of mRNA-SANPs. Non-statistically significant differences in toxicity were observed for cells transfected with 200 and 500 ng/mL (ns). Data are shown as mean ± SD of $N = 3$ independent replicates.

Materials (ASTM) measures hemoglobin content released from red blood cells upon nanoparticle-induced lysis. This assay is widely used due to its good reproducibility and low cost.[26] According to the ASTM standard, a hemolytic activity < 2% or between 2% and 5% can be regarded as non-toxic or mildly toxic, respectively. mRNA-SANPs exhibited a hemolytic activity of 1.22 (0.2) %, supporting their suitability for intravenous administration (Figure 2B).

SANP-mediated *in vitro* transfection

We further investigated the aforementioned mRNA eGFP-SANP platform *in vitro* using fluorescence/brightfield microscopy and a cytotoxicity assay. After assembly, 200 ng/mL of mRNA eGFP-SANP was used to transfect a monolayer of adherent HeLa cells in the presence of 10% fetal bovine serum (FBS). Lipofectamine 3000-eGFP mRNA and non-transfected cells served as controls. High transfection efficiency was achieved upon cell incubation with mRNA eGFP-SANP (Figure 3A), which is in good agreement with the fluorescence-activated cell sorting (FACS) analysis results shown in Figure S3. We next assessed SANP cytotoxicity at three different doses—200, 500, and 1000 ng/mL—by measuring cell viability using the GUAVA ViaCount assay on a Cytek Guava Muse Cell Analyzer. No dose-limiting toxicity was observed at 200 and 500 ng/mL; even the 1000 ng/mL dosage did not reach statistical significance, although it approached it, with a p value of 0.054 (Figure 3B). These results demonstrate that SANP formulations efficiently transduced large synthetic mRNA molecules in cultured cells without toxicity at physiological dosages, enabling *in vivo* testing of protein expression.

SANP-mediated mRNA transduction *in vivo*

We next investigated the *in vivo* transduction efficiency of mRNA-SANPs by IM and IV administration in mice using secreted embryonic alkaline phosphatase (SEAP) as a reporter gene. Sera from injected mice were collected after 3, 7, and 10 days, while a group of PBS-injected mice was used as a control. Potent SEAP translation was measured on day 3 for both IM- and IV-injected mice, followed by a gradual decrease in expression on days 7 and 10 (Figure 4).

Scratching, piloerection, and weight loss were monitored for up to 3 weeks, with no signs of toxicity observed in treated mice. To further assess the safety profile, plasma was collected 72 h and 7 days after IM and IV injections. Blood levels of glutamate oxaloacetate transaminase (GOT) and glutamate pyruvate transaminase (GPT) were measured as liver injury markers, while creatinine levels were assessed as a renal toxicity marker; PBS-treated mice served as controls (Figures 5A–5C). Notably, no increase in liver or renal injury markers was detected following either IV or IM administration of mRNA-SANPs. Additionally, no increase in the expression of inflammatory cytokines (interleukin-6 (IL-6) and tumor necrosis factor-alpha (TNF-α)) in serum was detected by ELISA 3 days post-injection (Figures 5D and 5E). Collectively, these data suggest that mRNA-SANP formulations are safe and do not induce systemic toxicity.

Analysis of mRNA-SANP PC and *in vivo* biodistribution

The *in vivo* administration of nanoparticles leads to the adsorption of serum proteins on their surface, forming the so-called PC, which

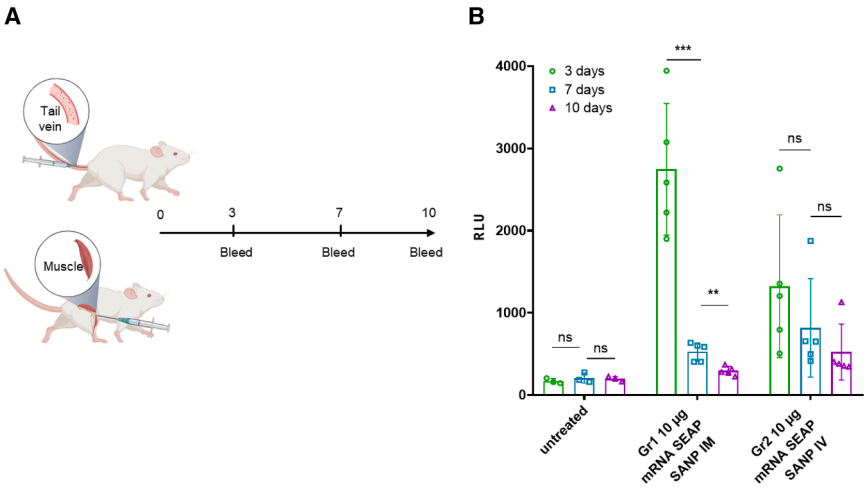

Figure 4. *In vivo* transduction of an mRNA-encoded reporter protein delivered by SANPs

(A) Treatment schedule: mice (n = 5/group) were administered 10 µg of mRNA SEAP-SANPs via tail vein or IM injection; mice were bled on days 3, 7, and 10 post-treatment. (B) Quantitative analysis of SEAP reporter gene levels in mice sera following IM or IV injection. Each dot represents an individual mouse serum at the given time point. Statistical analysis is reported as ns for non-statistically significant results; ** for $p < 0.005$; *** for $p < 0.0005$.

represents the actual interface between drugs and tissues.[27,28] It is well known that the PC influences nanoparticle colloidal stability in biological fluids, circulation half-life, and biodistribution. In turn, this can affect the nanoparticle ability to effectively deliver its payload and its toxicity.[29] To gain insights into the *in vivo* behavior of mRNA-SANP formulations, we carried out a compositional analysis of the mRNA-SANP PC. mRNA-SANPs were incubated with mouse sera for 1 h, as a plateau in protein-nanoparticle interactions is typically reached within this time frame. The PC was analyzed by mass spectrometry, as reported in the materials and methods section.

A total of 1,692 proteins were identified in the mRNA-SANP PC. In particular, proteins with a molecular weight between 30 and 70 kDa represented the most abundant fraction, comprising about 45% of the total PC. Proteins in the 1–30 kDa and 70–150 kDa ranges were equally enriched on SANPs, while interactors with a molecular weight over 150 kDa were the least represented, with only 107 proteins detected (Figures 6A and 6B). The top 30 enriched proteins on the mRNA-SANP surface are reported in Table S1. The SANP PC was enriched with specific serum proteins, suggesting the occurrence of well-defined interactions between SANPs and serum proteins. As an example, in Balb/c mice, albumin comprises between 46% and 58% of total serum protein,[30] whereas the top proteins present in the SANP PC are apolipoprotein C-III, a member of the apolipoprotein family responsible for lipid transport in circulation,[31] vitronectin, serum paraoxonase/arylesterase 1, albumin, and apolipoprotein AI (Table S1).

To understand how the PC determines the ultimate fate of SANPs *in vivo*, we carried out a biodistribution experiment. Briefly, mRNA encoding firefly luciferase was produced and encapsulated into SANPs; 10 µg of SANP-encapsulated luciferase mRNA were then injected in mice *via* the IM or IV route. The day after administration, the *in vivo* imaging system (IVIS) was used to measure luciferase expression in mice. We observed luciferase expression at the injection site in mice that received mRNA-SANPs *via* the IM route, while luciferase was mainly detected in the lungs of mice that were administered mRNA-SANPs *via* IV injection (Figure 6C). *Ex vivo* imaging of organs (i.e., liver, heart, lung, kidney, and muscle) demonstrated NP accumulation in the lungs and complete exclusion from the liver (Figure S4).

Genetic vaccination with mRNA-SANP

We then evaluated the potential of mRNA-SANPs as a genetic vaccine delivery platform using the SARS-CoV-2 spike protein as a model antigen[32] and explored both the IM and IV routes for vaccination. Six-week-old female BALB/c mice were immunized with mRNA Spike-SANPs using a homologous prime-boost regimen, receiving two injections of 10 µg each at 0 and 4 weeks. The B and T cell immune responses were measured 10 days after the boost dose. The T cell response was assessed using an interferon (IFN)-γ ELISpot assay following *ex vivo* pulsing of splenocytes with two separate peptide pools covering the entire spike protein: subunit 1 (S1: amino acids 1–686) and subunit 2 (S2: amino acids 687–1273). Both the IM and IV administration routes were equally effective, with all mice developing a potent T cell response, averaging approximately 500 spot-forming cells per million splenocytes. Consistent with previous reports for this mouse strain, the response to the S1 pool was higher than the response to the S2 pool (Figure 7).[33] The humoral response to the vaccine was analyzed using an anti-Spike ELISA. Interestingly, a statistically significant difference was observed between the two delivery routes, with IV vaccination inducing consistently higher antibody titers compared to IM vaccination (Figure 8).

DISCUSSION

The success of COVID-19 mRNA genetic vaccines has renewed interest in developing mRNA formulated into lipid-based nanoparticles as vectors for anti-infectious and anti-cancer immunotherapies, as well as gene therapy applications. However, current mRNA formulations suffer from poor stability during long-term storage, highlighting the need for alternative approaches. In this context, the development of

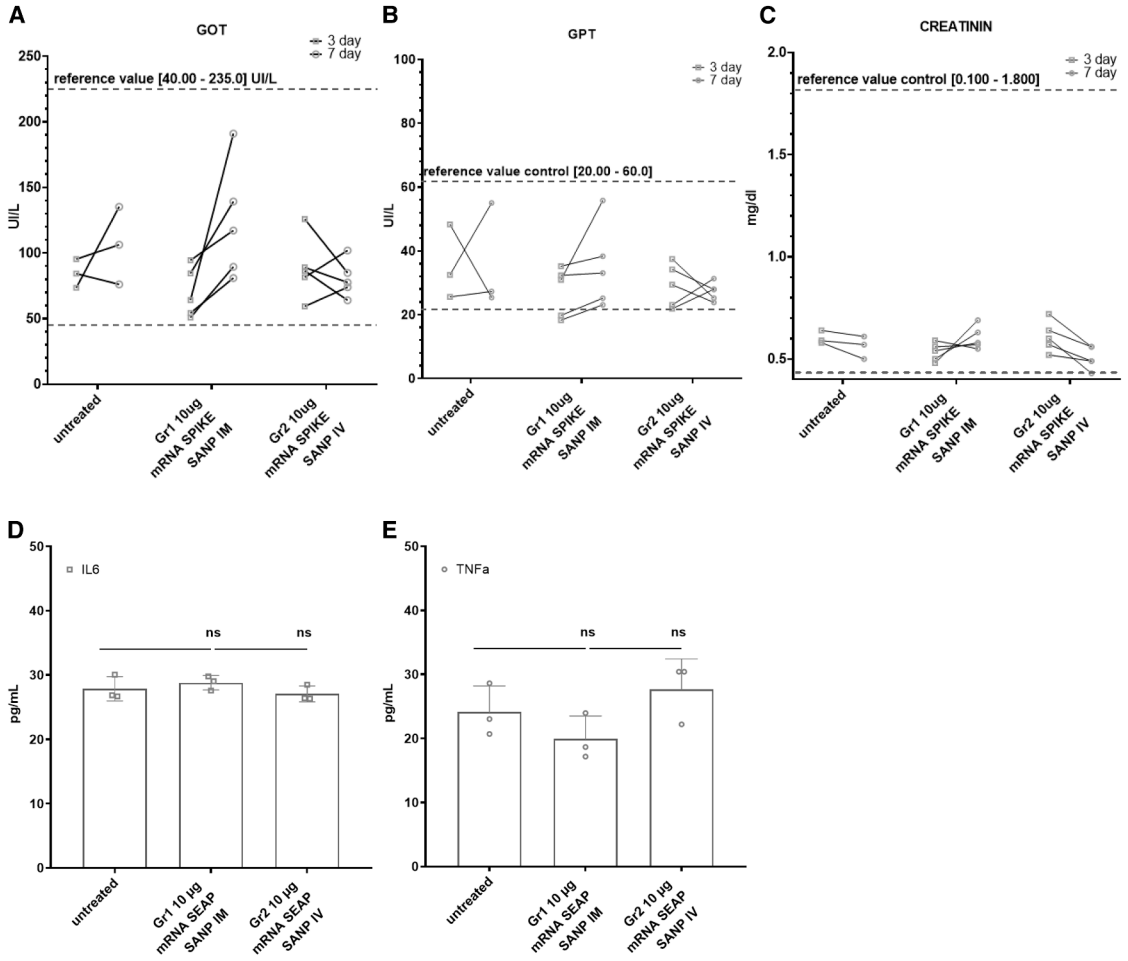

Figure 5. Assessment of systemic toxicity of mRNA-SANPs

Liver and renal toxicity were assessed by measuring the GOT (A), GPT (B), and creatinine (C) levels. Dashed lines indicate the reference values for healthy mice. Untreated mice (n = 3); mRNA-SANPs IM (n = 5); mRNA-SANPs IV (n = 5). Squares represent values for individual mice on day 3, and circles represent values on day 7. No statistically significant differences were reported. IL-6 (D) and TNF-alpha (E) were also assessed at day 3 post-injection. Each square represents the value for a single mouse. Untreated mice (n = 3); mRNA-SANPs IM (n = 3); mRNA-SANPs IV (n = 3). No statistically significant differences were reported.

mRNA-based formulations that can be assembled at the point of care may be a viable strategy. Recent work from Tanaka et al. introduced a post-encapsulation method to load mRNA into pre-formed LNPs, which induced mRNA expression *in vitro* and *in vivo*.[34] Whilst very elegant, the method reported by Tanaka et al. has some limitations, mainly associated with poor flexibility in terms of lipid composition and the need to use high N/P ratios (e.g., 16).

We previously developed a nanoparticle platform technology, referred to as SANP, consisting of three main components: CaP NPs, RNA oligonucleotides, and cationic liposomes with varying lipid composition. These components can be stored at 4°C and mixed immediately before use in clinical settings. In this work, we tailored the SANP technology for the formulation of large synthetic mRNA, leveraging its simplicity of preparation and long-term stability at 4°C, with potential clinical applications in genetic vaccination, gene replacement, and gene editing using exogenous molecular scissors, such as Cas9. We successfully generated mRNA-loaded SANPs with hydrodynamic diameters below 200 nm, low PDI, positive surface charges, mRNA encapsulation efficiencies exceeding 98%, good colloidal stability post-assembly and in human plasma, and low hemolytic activity.

SANPs encapsulating reporter genes mRNAs efficiently transduced cells and tissues *in vitro* without signs of cytotoxicity. In particular, SANPs exhibited a similar transfection efficacy to Lipofectamine, which is encouraging given that Lipofectamine 3000 is a gold-standard reagent for *in vitro* transfection studies, whereas SANPs are primarily designed for *in vivo* applications. The transfection efficacy of SANPs stored at 4 °C was retained after 7 days, while a 20% reduction was observed after 14 days. This decrease in transfection ability may be due to mRNA degradation[35] rather than to changes in SANP formulation, as the colloidal properties remained unchanged over

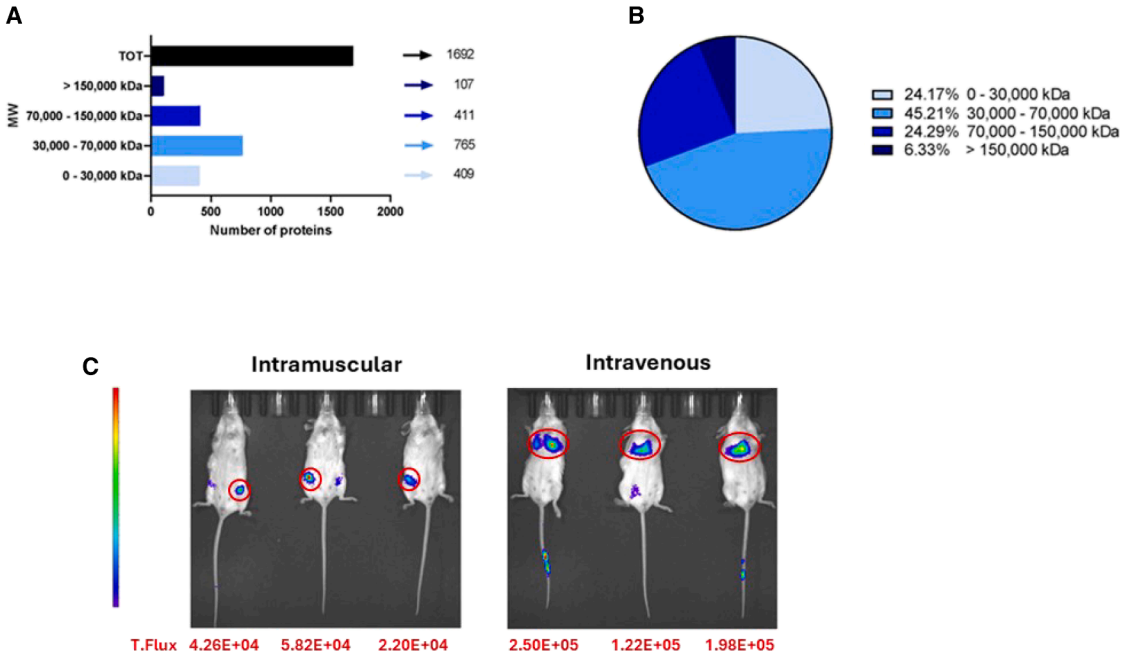

Figure 6. mRNA-SANP protein corona characterization and *in vivo* biodistribution

mRNA SEAP-SANPs were incubated with mouse serum, and the protein corona was evaluated by mass spectrometry. (A) Distribution of protein corona composition according to protein molecular weight. (B) Pie chart reporting the data from (A) as percentage composition. (C) *In vivo* biodistribution of mRNA luciferase-SANPs, determined 16 h post-injection in $n = 3$ mice for the IM group and $n = 3$ mice for the IV group.

this time frame. It is worth mentioning that the SANP platform has been devised as a "just-before-use" formulation, with its components to be mixed at the point of care before administration. We then probed the *in vivo* transduction efficiency of mRNA-SANPs in mice using SEAP as a reporter gene. Following both IM and IV administration in mice, translation of SANP-encapsulated SEAP mRNA was sustained for up to 7 days, with no liver or renal toxicity or systemic inflammatory response.

A compositional analysis of the PC adsorbed onto the surface of mRNA-SANPs after serum incubation identified a subset of serum proteins that preferentially accumulated on the nanoparticle surface, including members of the apolipoprotein family, vitronectin, and albumin. Interestingly, the preferential adsorption of apolipoprotein C-III on the surface of cationic LNPs has been recently shown to improve nanoparticle uptake by mouse bone marrow-derived mast cells,[36] suggesting potential future applications of SANP technology in specific clinical settings. The abundance of vitronectin in the mRNA-SANP PC was not surprising, given the presence of cationic lipids in the nanoparticle composition,[37] while the presence of albumin and apolipoprotein AI among the 10 most abundant proteins could be explained by their abundance in serum.[38] We corroborated the PC data with biodistribution studies on SANPs loaded with luciferase-encoding mRNA following IM and IV administration. While mRNA expression was localized at the injection site for mRNA-SANPs administered *via* the IM route, SANP-mediated luciferase expression was observed predominantly in the lungs when the IV route was used. This phenomenon may be ascribed to the abundance of vitronectin in the PC of SANPs, which mediates lung targeting due to the expression of vitronectin receptors by lung endothelial cells.[39]

As a proof of concept for the clinical application of mRNA-SANP technology, we evaluated its ability to induce an immune response against the SARS-CoV-2 spike protein following IM or IV administration in mice. Both routes of administration elicited strong antigen-specific T and B cell immune responses, with IV vaccination yielding a significantly stronger humoral response than IM vaccination. Overall, we successfully developed a novel lipid-based nanoparticle formulation for mRNA delivery, offering potential for rapid clinical translation due to its straightforward assembly, convenient storage stability, favorable safety profile, and significant *in vivo* transduction efficiency. Future studies will focus on expanding the applicability of the mRNA-SANP platform for therapeutic anti-cancer vaccines and gene replacement therapies.

MATERIALS AND METHODS

Materials

Calcium chloride ($CaCl_2$), sodium chloride (NaCl), and sodium phosphate dibasic (Na_2HPO_4) were purchased from Merk Life Science S.r.l. (Milan, Italy). DOTAP was kindly provided by Lipoid GmbH (Ludwigshafen, Germany) while Cer_{16}-PEG_{2000} was purchased from Avanti Polar Lipids (Alabaster, USA). Regenerated cellulose syringe filters with a 0.2 μm pore size were purchased from Exacta+Optech Labcenter SpA (San Prospero, Italy). The Quant-iT

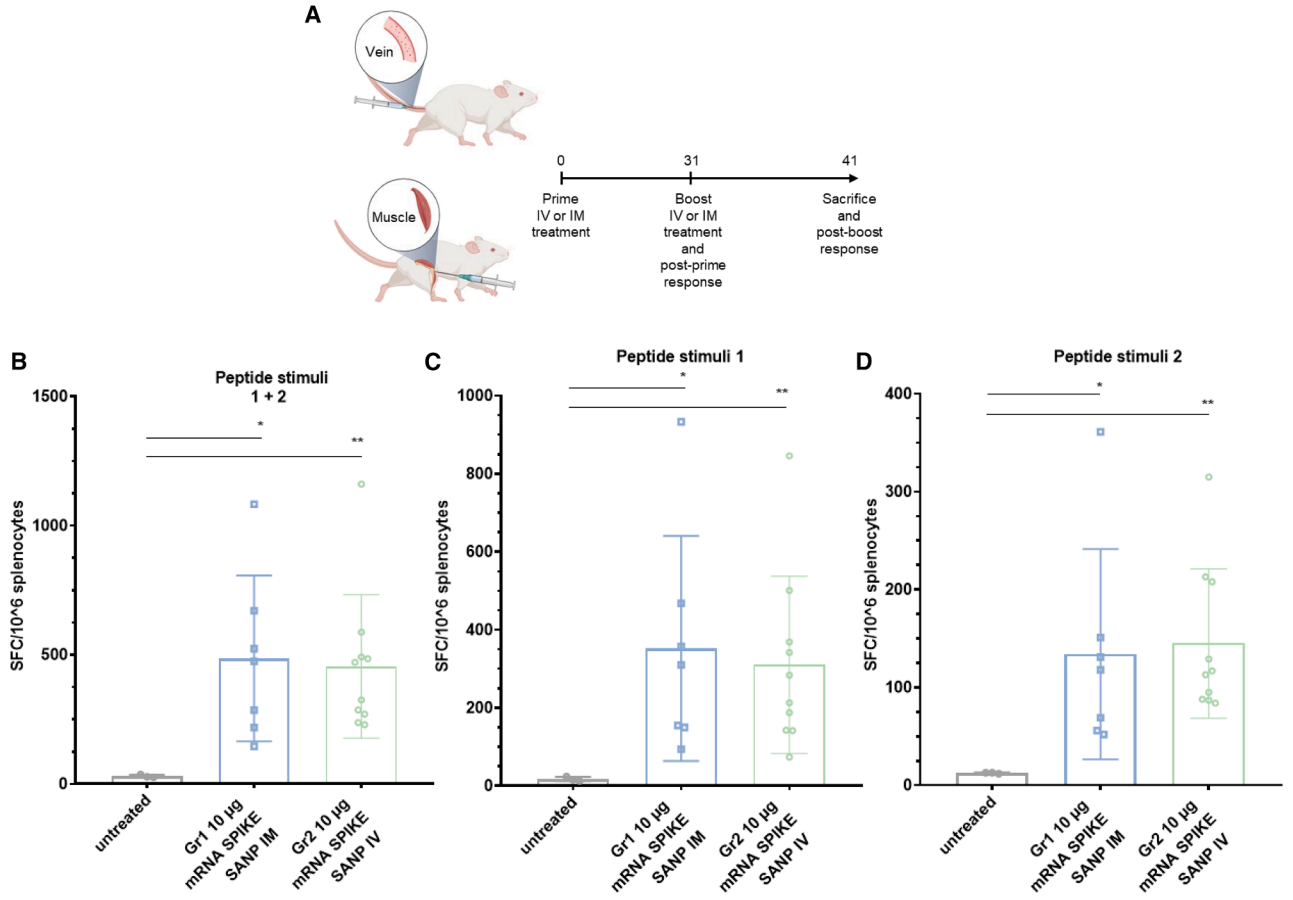

Figure 7. Anti-spike T cell immune response

(A) Timeline of treatment. Mice were immunized on day 0 and day 30 with 10 µg mRNA Spike-SANP following a prime-boost regimen. Spleens were collected on day 40, 10 days after the boost injection. SFC/10 ^{6} splenocytes was calculated by ELISPOT assay. The sum of anti-S1 and anti-S2 T cell response is shown in (B). Separate S1 or S2 responses are shown in (C) and (D), respectively. Each dot represents an independent mouse. Untreated $n = 7$, Spike-SANPs IM $n = 9$, Spike-SANPs IV $n = 9$. Statistical analyses were reported as ** for $p < 0.005$ and *** for $p < 0.0005$. Part of the figure was created using Biorender.

RiboGreen RNA Assay was purchased from Thermo Fisher Scientific (Milan, Italy). Maxiprep of IVT plasmid were performed using the EndoFree Plasmid Maxi Kit (Quiagen, Hilden, Germany). The IVT plasmid was linearized with LguI (SapI), purchased from Thermo Fisher Scientific (Milan, Italy). *In vitro* transcription was performed using the T7 Flashscribe Kit from CellScript (Post Rd, Madison, USA) in the presence of CleanCap Reagent (3′ OMe) AG CAP1 and N1-Methylpseudouridine-5′-triphosphate from TriLink (San Diego, USA). IVT mRNA was purified by affinity chromatography using POROS Oligo(dT)25 Affinity Resin purchased from Thermo Fisher Scientific (Milan, Italy). Water and acetonitrile (liquid chromatography-mass spectrometry [LC-MS] grade, LiChrosolv) were purchased from Merck KGaA (Darmstadt, Germany). Ammonium bicarbonate (NH_4HCO_3), DL-dithiothreitol (DTT), and iodoacetamide (IAA) and trypsin (porcine pancreas-derived) were purchased from Sigma-Aldrich (Buchs, Switzerland). Trifluoroacetic acid (TFA) was obtained from Honeywell SC (Seeelze, Germany). Formic acid (FA, LiChropur) was purchased from Merck KGaA (Darmstadt, Germany). Pierce HeLa protein digest standard was obtained from Thermo Fisher Scientific (Waltham, MA, USA), and the MMI-L low-concentration tuning mix was purchased from Agilent Technologies (Santa Clara, CA, USA).

Methods

CaP NPs preparation

CaP NPs were prepared by dropwise mixing equal volumes of Na_2HPO_4 (10.8 mM, pH 9.5) and $CaCl_2$ (18 mM, pH 9.5) aqueous solutions in a 1:1 (v/v) ratio under stirring at 1400 rpm. The resulting suspension was stirred for an additional 10 min and filtered through 0.22 µm pore-sized polycarbonate filters. The CaP NPs were stored at 4°C until further use.

Liposome formulation

Liposomes (DOTAP:$Cer_{16}PEG_{2000}$ = 94:6 mol%) were prepared using the thin-film hydration method followed by extrusion. DOTAP and $Cer_{16}PEG_{2000}$ were dissolved in a chloroform:methanol mixture

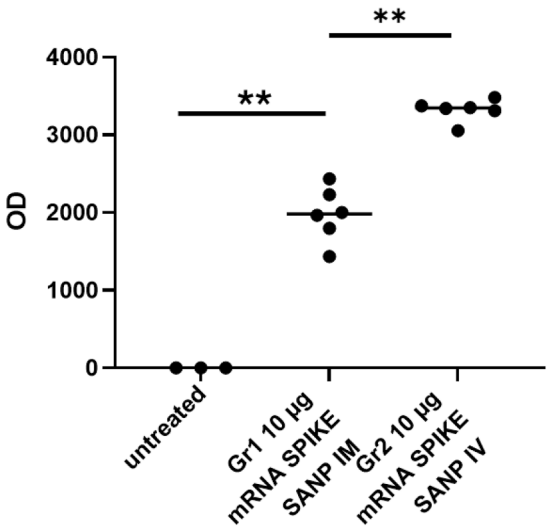

Figure 8. B cell response against the spike protein

Antibody titers were calculated in the sera of immunized mice, with each dot representing an individual mouse. Untreated group $n = 3$; IM- and IV-injected groups $n = 6$ each. Statistical analysis was performed by comparing line-matched groups using the Student's t test. ** for $p < 0.005$.

(2:1 v/v) and transferred to a 50 mL round-bottom flask. The organic solvent was removed by rotary evaporation (Laborata 4010 digital, Heidolph, Schwabach, Germany), and the resulting lipid film was hydrated with RNAse-free water for 2 h at 65°C. The vesicle suspension was extruded through pore-sized polycarbonate membranes (Nucleopore Track-Etched, 25 mm, Whatman, Brentford, UK) using a thermobarrel extruder (Lipex Extruder, Evonik, Essen, Germany) operated at 65°C. The liposomes were sequentially extruded through 400 nm membranes (3 passages), 200 nm membranes (3 passages), and 100 nm membranes (5 passages). The liposomes were stored at 4°C until further use.

mRNA-SANP preparation

mRNA-loaded SANP formulations were prepared by mixing IVT mRNA in aqueous solution (1 mg/mL) with an aqueous NaCl solution and CaP NPs at a 1:1.2 (v/v) ratios. The suspension was vortexed at 800 rpm for 5 s and incubated at room temperature for 10 min. The resulting CaP-mRNA complexes were then combined with liposomes at a 1:1.3 (v/v) ratio (N/P = 9) and incubated at room temperature for 25 min. The final mRNA concentration in the formulation was 200 µg/mL, while the NaCl concentration was 150 mM. The concentration of formulated mRNA was determined by measuring the amount of unencapsulated mRNA *via* the Quant-iT RiboGreen RNA Assay and a mRNA standard curve ($R^2 = 0.99$). The mRNA encapsulation efficiency was determined as:

$$Encapsulation\ efficiency = \frac{[mRNA]_{total} - [mRNA]_{buffer}}{[mRNA]_{total}} * 100, \quad \text{(Equation 1)}$$

where $[mRNA]_{total}$ is the total mRNA concentration in the formulation and $[mRNA]_{buffer}$ is the concentration of unencapsulated mRNA.

NP physicochemical characterization

Formulations were characterized in terms of colloidal dimensions, PDI, and surface charge using DLS (Zetasizer Nano Z, Malvern, UK). For each formulation, the z-average diameter, PDI, and zeta potential were calculated as mean ± standard deviation from measurements obtained from three independent batches.

Stability of mRNA-SANP in biological media

The colloidal stability of mRNA-SANP formulations against aggregation upon dilution in human plasma was measured *via* DLS. Whole blood was centrifuged at 2000 rpm for 15 min (MIKRO 20; Hettich, Tuttlingen, Germany) to separate erythrocytes from plasma. The collected plasma was diluted to 1% in phosphate buffer (136 mM NaCl, 27 mM KCl, 8 mM Na_2HPO_4, 2 mM KH_2PO_4, 1× PBS) at pH 7.4. mRNA-SANP formulations were incubated in a 1% plasma solution at 37°C at a final mRNA concentration of 20 µg/mL, and the mean hydrodynamic diameter of the formulations was measured at various time points by DLS. mRNA-SANPs incubated in PBS were used as controls.

Hemolysis assay

Hemolysis assays on mRNA-SANPs were performed on fresh blood according to a previously published protocol.[21] Erythrocytes were isolated from plasma by centrifugation at 2000 rpm for 15 min (MIKRO 20; Hettich, Tuttlingen, Germany) and resuspended in a 150 mM NaCl solution. The resuspended erythrocytes were subjected to three additional centrifugation and reconstitution steps to remove residual plasma; they were then diluted 1:10 (v/v) in 150 mM NaCl. mRNA-SANP formulations were added to the erythrocytes at 0.2% (w/v) and incubated for 4 h at 37°C. The samples were placed on ice for 2 min to stop erythrocytes lysis and centrifuged twice (3000 rpm, 5 min) to retrieve the supernatant. The free hemoglobin content was determined by measuring the absorbance of the supernatants at 540 nm (Thermo Fisher Scientific, 1510 Multiskan Go). Erythrocytes diluted in 150 mM NaCl or water were used as the 0% and 100% hemolysis controls, respectively. The hemolysis percentage was calculated using the following formula:

$$Hemolysis\ \% = \frac{(Abs_{sample} - Abs_{0\%})}{(Abs_{100\%} - Abs_{0\%})} * 100, \quad \text{(Equation 2)}$$

where Abs_{sample} is the absorbance of the sample, $Abs_{0\%}$ is the absorbance at 0% hemolysis, and $Abs_{100\%}$ is the absorbance at 100% hemolysis.

Cryogenic TEM

To obtain images of the colloidal structures, mRNA-SANPs were freshly prepared at a concentration of 200 µg/mL as described above. Ultrathin carbon films mounted on Cu 200 mesh grids

(Agar Scientific, UK) served as substrates for sample deposition. The grids were first plasma-treated at 230 V under a 0.15 mbar vacuum for 5 s. A 4 μL aliquot of the sample was then pipetted onto the front side of the prepared grids. The blotting chamber was preconditioned to 21°C and 90% humidity. Samples were plunge-frozen using a Vitrobot (FEI, USA). Following a 30 s rest in the chamber, excess liquid was automatically blotted away using two strips of filter paper with a blot time of 1 × 1.5 s, and the grids were immediately plunge-frozen into liquid ethane maintained at −180°C. The prepared grids were stored in liquid nitrogen until TEM analysis. Low-dose electron diffraction studies were performed using an FEI Tecnai Spirit F20 electron microscope (FEI, USA) operated at 80 kV, and images were recorded with an FEI Eagle CCD camera (FEI, USA).

In vitro *transcription of mRNA*

The coding sequences for eGFP, SEAP, firefly luciferase, and SARS-CoV-2 spike were mouse codon optimized. Templates for *in vitro* transcription were generated by cloning synthetic double-stranded DNA (dsDNA) strings into the pMA7 plasmid downstream of the T7 AGG promoter and upstream of the 3′ untranslated region (UTR) comprising Tle5 and mtRNR UTRs. A co-transcriptional poly(A) tail was ensured by incorporating into the template DNA a segmented 100-nt poly(A) stretch upstream of the LguI restriction site. Briefly, after plasmid DNA was linearized, 1 μg of template was transcribed according to the T7 Flash Scribe kit manufacturer's instructions. Uridine was 100% replaced with N1-methylpseudouridine-5′-triphosphate. The *in vitro* transcription reaction was incubated for 2 h at 37°C. DNase was then added and incubated for 15 min. The resulting IVT mRNA was purified by affinity chromatography using oligo(dT) resin, according to manufacturer's instructions. RNA purity and a monodispersed peak were confirmed by capillary electrophoresis (TapeStation), and quantification was performed using Qubit.

mRNA-SANP in vitro *activity*

FACS analysis was performed at the CEINGE in-house facility as previously reported.[40] A total of 1.10 × 10^5 HeLa cells were seeded in a 12 multi-well plate and, 24 h later, transfected with eGFP mRNA formulated with either Lipofectamine or SANPs, as described in the mRNA-SANP preparation section. After 24 h, cells were detached using PBS containing 5 mM EDTA and washed three times with PBS. eGFP expression was assessed and monitored using a Becton Dickinson FACSAria cell sorter. To assess cell viability, the Guava ViaCount reagent was used to differentiate viable and non-viable cells, utilizing two DNA-binding dyes with distinct permeability properties. One dye selectively stains nucleated cells, while the other highlights dying cells. This unique dye combination allows Guava ViaCount to effectively distinguish viable, apoptotic, and dead cells. Stained cells were analyzed using a Cytek Guava Muse Cell Analyzer according to the manufacturer's instructions.

mRNA-SANP in vivo *activity*

All animal studies were approved by Italian ministry of health (n° 589/2024-PR). Six-week-old female BALB/c mice were used for *in vivo* experiments. Total volumes of 50 and 100 μL were used for IM and IV injection of mRNA-SANP formulations, respectively. To monitor the activity of the SEAP reporter gene, mice received 10 μg of mRNA SEAP-SANPs via IM or tail vein injection. Sera were collected at the indicated time points, and SEAP expression was assessed using the Tropix Phospha-Light assay, as previously reported.[41] In order to investigate the anti-spike immune response, mice were administered 10 μg of mRNA Spike-SANPs in a prime-boost regimen (0 and 30 days after the first injection) *via* IM or IV injection.

The biochemical analysis of mouse sera was performed using the BT3500 analyzer (Biotecnica Instruments S.p.A.) with the following reagents, according to the manufacturer's instructions: GOT-AST UV IFCC (product reference: ASSL-0430, Elitech), GPT-ALT UV IFCC (product reference: ALSL-0430, Elitech), UREA assay (product reference: URSL- 0427, Elitech), and creatinine assay (product reference: BT164L SGM). IL-6 and TNF-α were measured in mouse sera using ELISA kits (IL-6 product reference: M6000B-1, R&D Systems Inc; TNF-α product reference: MTA00B-1, R&D Systems Inc.), according to the manufacturer's instructions. Biodistribution experiments were performed by administering 10 μg of mRNA luciferase-SANPs *via* IM or IV injection in mice. Sixteen hours post-injection, mice received D-luciferin substrate, and *in vivo* bioluminescence imaging was performed using an IVIS Spectrum system under anesthesia.

The T and B cell response were measured using ELISpot and ELISA assays, respectively, as previously reported.[42,43] Briefly, T cell responses were assessed using the ELISpot assay. MultiScreen HTS Immobilon-P 96-well plates (product reference: MSIPS4510, Merck Life Science S.r.l.) were coated with 10 μg/mL of anti-mouse IFN-γ antibody (product reference: CT665-C, U-CyTech biosciences) and incubated overnight at 4°C. After washing and blocking the plates, lymphocytes freshly isolated from mouse spleens were plated in duplicate at two cell densities (2.5 × 10^5 and 5 × 10^5 cells) and stimulated for 18 h at 37°C with 5% CO_2 using peptides. S1 or S2 (product reference: JPT PepMix; JPT Peptide Technologies GmbH) 15-mer peptide pools, overlapping by 11 amino acid residues and covering the entire SARS-CoV-2 spike protein, were used at a final concentration of 1 μg/mL. Dimethyl sulfoxide (DMSO, product reference: D2650, Merck Life Science S.r.l.) and concanavalin A (ConA, product reference: C5275, Merck Life Science S.r.l.) were used as negative and positive controls, respectively. Cells were then washed away, and the plates were incubated with biotinylated anti-mouse IFN-γ antibody (dilution 1:100, product reference: CT665-C, U-CyTech biosciences), followed by streptavidin-alkaline phosphatase (dilution 1:2500, product reference: 554065, BD Biosciences), and treated with a 5-bromo-4-chloro-3-indoyl-phosphate/nitro blue tetrazolium 1-Step solution (BCIP/NBT, product reference: 34042, Thermo Fisher Scientific). The addition of an insoluble alkaline phosphatase substrate resulted in the appearance of dark spots in the wells at the sites where the cells were located, with the one spot representing each T cell that secreted IFN-γ. The number

of spots per well could be directly related to the precursor frequency of antigen-specific T cells. Plates were counted and analyzed using a CTL ImmunoSpot reader (ImmunoSpot, OH, USA). ELISpot data responses were expressed as cytokine IFN-γ spot forming cells (SFCs) per million splenocytes, after subtraction of the DMSO background.

Sera were analyzed by ELISA; a custom SARS-CoV-2 ELISA was developed using His-tagged protein immobilized on Ni-NTA His-Sorb strips or plates (product reference: 15162, Qiagen). This assay employed a His-tagged full-length SARS-CoV-2 spike protein produced in baculovirus (product reference: 40589-V08B1, Sino Biological). An optimized protein concentration (1 μg/mL for the full-length Spike) in a 100 μL volume was applied to Ni-NTA plates or strips and incubated for 1 h at 25°C with shaking. Diluted sera were then added and incubated for 2 h at 25°C with continuous agitation. Binding was detected using alkaline phosphatase-conjugated secondary antibodies, including anti-mouse total immunoglobulinG (IgG) (product reference: A3562, Merck Life Science S.r.l.), along with anti-mouse IgG1 (product reference: 550878, BD Biosciences) and IgG2a (product reference: 553501, BD Biosciences). The alkaline phosphatase substrate was prepared by dissolving SigmaFast tablets (product reference: S0942, Merck Life Science S.r.l.) in sterile distilled water (product reference: 15230-147, Gibco). Absorbance readings were taken at 405 and 620 nm using an EnSight multimode plate reader (PerkinElmer, Waltham, MA, USA).

PC formation

PCs were obtained as previously described.[44,45] Briefly, SANPs (1 mg/mL lipid concentration) were incubated with mouse serum (6-week-old female BALB/c) at a 1:1 v/v ratio at 37°C for 1 h under constant agitation (500 rpm) (Eppendorf ThermoMixer C, Sigma-Aldrich, St. Louis, MO, USA). After incubation, SANPs were centrifugated for 30 min at 14,000 rpm and 10°C. The resulting pellet was washed three times with 200 μL of ice-cold PBS to remove the soft corona. The PC was then eluted from the NPs using a denaturation buffer (8 M urea and 50 mM NH_4HCO_3). Proteins within the corona were quantified by Bradford assay (Bio-Rad, Segrate (MI), Italy) using bovine serum albumin at known concentrations to build 5-point standard curve (R^2 = 0.99). PCs were stored at −20°C until mass spectrometry analysis. Prior to incubation with SANP, serum was centrifuged at 14000 × g to remove potential protein aggregates, and the collected supernatant was used for PC formation.

Mass spectrometry analysis

For sample preparation, NP extracts were prepared using S-trap TM Micro spin columns (Protifi) according to the manufacturer's instructions, with slight adjustments.[46] Tris-phosphate was used in place of triethylammonium bicarbonate (TEAB) buffer both in the sodium dodecyl sulfate (SDS) lysis buffer (10% SDS, 100 mM tris-phosphate, pH 8.5) and in the binding buffer (90% aqueous methanol with a final concentration of 100 mM tris-phosphate, pH 7.55), while NH_4HCO_3 was used as the digestion buffer (50 mM NH_4HCO_3). Briefly, 22 μg of SANPs were diluted with an equal volume of lysis buffer. Disulphide bonds were then reduced using 20 mM DTT for 45 min at 56°C and alkylated with 40 mM IAA for 30 min in the dark. Aqueous phosphoric acid was added to a final concentration of 1.2%, followed by the binding buffer at a 1:6 (v/v) ratio. The mixture was loaded into the micro-column for protein trapping and trypsinization (2.2 μg per sample) following the manufacturer's protocol. After overnight incubation at 37°C, peptides were eluted by centrifugation at 4,000 × g with 40 μL of 50 mM NH_4HCO_3, ollowed by 40 μL of 0.2% FA. Hydrophobic peptides were recovered with 40 μL of 50% acetonitrile. The pooled eluates of each sample were dried and resuspended in 25 μL of 0.1% FA. Peptide content was quantified using a Nanodrop spectrophotometer (NanoDrop OneC, Thermo Fisher Scientific, Wilmington, DE, USA).

LC-MS/MS analysis

Digests were injected into an Evosep One (Evosep Biosystems, Odense, Denmark) LC system coupled online with a timsTOF fleXTM (Bruker Daltonics, Bremen, Germany) mass spectrometer, as reported in the literature, with some modifications.[47] Peptides were loaded onto a disposable trap column, Evotip PureTM (Evosep Biosystems, Odense, Denmark), following the manufacturer's protocol. Desalted and concentrated peptides were separated on an analytical 8 cm column (PepSep C18, 8 cm Performance column, particle size 1.5 μm, internal diameter 150 μm) at 40°C. A gradient of solvent A (0.1% FA) and solvent B (acetonitrile (ACN), LC-MS grade, LiChrosolv, + 0.1% FA) was applied over 21 min (60 sample per day (SPD)) for the separation. The eluted peptides were ionized using a nanoBoosterCaptiveSpray (Bruker Daltonics). The mass spectrometer was operated in DIA (data independent acquisition)-PASEF (parallel accumulation-serial fragmentation) mode. Ions were scanned in positive mode over an m/z range of 100–1700, with an energy ramping mobility range of 0.85–1.30 V·s/cm^2. The dry gas flow was 3.0 L/min at 180°C, and the capillary voltage was 1,400 V. For tandem mass PASEF analysis, clusters of mono-charged ions were excluded to reduce the complexity of tandem mass spectrometry (MS2) spectra using the following parameters: m/z 348.1–973.1 Da and 0.80–1.22 1/K0. The estimated cycle time for each PASEF analysis was 1.17 s, with a total of 10 cycles using DIA windows of 25 Da. The mass spectrometer was calibrated for mass and ion mobility accuracy using a mixture of ten standards with known masses (MMI-L Low Concentration Tuning Mix, Agilent Technologies, Santa Clara, CA, USA). For calibration on the nano-source, three specific lock masses (622.0290 m/z, 922.0098 m/z, and 1221.9906 m/z) were applied through a filter. Raw data were processed using SpectronautTM (v.18.1, https://biognosys.com) following a library-free processing method based on the Mus Musculus (Swissprot, downloaded on 12-05-2023, 17155 entries) database. The parameters were set as follows: trypsin as the enzyme, carbamidomethyl (C) as a fixed modifications, and acetylation (protein N-term) and oxidation (M) as variable modifications, with 1% false

discovery rate (FDR) at the precursor and protein levels. Abundance values were automatically cross-run normalized. Proteins were considered identified only if they had at least one unique significant peptide.

Statistical analysis

Assuming that all samples and replicates were normally distributed, the Student's *t* test was used as a statistical method to determine whether there was a significant difference between the means of two groups. Statistical significance was shown as * for $p < 0.05$ and ** for $p < 0.005$. NS means not significant ($p > 0.05$).

DATA AND CODE AVAILABILITY

Data will be available upon request from the corresponding authors.

ACKNOWLEDGMENTS

This work was supported by a grant from the Phospholipid Research Center to G.D.R. (GDR-098/2-1); POR Campania: piattaforma per lo sviluppo di nuove tecnologie vaccinali; PNRR CN3 National Center for Gene Therapy and Drugs based on RNA Technology; PNRR PE13 One Health Basic and Translational Research Actions addressing Unmet Needs on Emerging Infectious Diseases; and PNRR-POC-2022-12375713. A.A. was supported by a Research Fellowship financed within POR Campania: piattaforma per lo sviluppo di nuove tecnologie vaccinali. Cryogenic electron microscopy sample preparation and imaging were performed with devices supported by the Microscopy Imaging Center (MIC) of the University of Bern. The *in vivo* studies were carried out under authorization n° 744/2024-PR (Risp. a prot. A69A0.144). Part of the schematics shown in this work was created using https://BioRender.com or by Servier Medical Art.

AUTHOR CONTRIBUTIONS

A.D.C.: Conceptualization, Data Curation, Formal analysis, Investigation, Methodology, Validation, Visualization, Writing – original draft, Writing – review & editing. V.N.: Conceptualization, Data Curation, Formal analysis, Investigation, Methodology, Validation, Visualization, Writing – original draft, Writing – review & editing. A.A.: Investigation, Validation. V.C.: Formal analysis, Data curation. A.C.: Investigation, Methodology, Validation. G.F.: Formal analysis, Investigation, Methodology, Validation, Visualization. A.S.: Investigation, Methodology, Validation. E.P.: Investigation, Methodology, Validation. A.G.: Formal analysis, Investigation, Methodology, Validation, Visualization. Clizia Chinello: Formal analysis, Investigation, Methodology, Validation, Visualization. L.P.: Formal analysis, Investigation, Methodology, Validation, Visualization. R.E.: Formal analysis, Investigation, Methodology, Writing – review & editing. P.L.: Resources, Funding acquisition, Supervision, Writing – review & editing. Claudia Corbo: Formal analysis, Investigation, Methodology, Validation, Visualization. A.N.: Conceptualization, Funding acquisition, Project administration, Supervision, Writing – review & editing. E.S.: Conceptualization, Funding acquisition, Project administration, Supervision, Writing – review & editing. G.D.R.: Conceptualization, Funding acquisition, Project administration, Supervision, Writing – review & editing.

DECLARATION OF INTERESTS

P.L. has consulted for Lipoid GmbH, Sanofi-Aventis Deutschland, and DSM Nutritional Products Ltd. And has received grants from Lipoid GmbH, Sanofi-Aventis Deutschland, DSM Nutritional Products Ltd., and PPM Services SA on unrelated projects.

SUPPLEMENTAL INFORMATION

Supplemental information can be found online at https://doi.org/10.1016/j.omtn.2026.102851.

REFERENCES

1. Jackson, L.A., Anderson, E.J., Rouphael, N.G., Roberts, P.C., Makhene, M., Coler, R.N., McCullough, M.P., Chappell, J.D., Denison, M.R., Stevens, L.J., et al. (2020). An mRNA Vaccine against SARS-CoV-2 — Preliminary Report. N. Engl. J. Med. *383*, 1920–1931. https://doi.org/10.1056/NEJMoa2022483.
2. Walsh, E.E., Frenck, R.W., Falsey, A.R., Kitchin, N., Absalon, J., Gurtman, A., Lockhart, S., Neuzil, K., Mulligan, M.J., Bailey, R., et al. (2020). Safety and Immunogenicity of Two RNA-Based Covid-19 Vaccine Candidates. N. Engl. J. Med. *383*, 2439–2450. https://doi.org/10.1056/NEJMoa2027906.
3. Pardi, N., Hogan, M.J., Porter, F.W., and Weissman, D. (2018). mRNA vaccines — a new era in vaccinology. Nat. Rev. Drug Discov. *17*, 261–279. https://doi.org/10.1038/nrd.2017.243.
4. Chaudhary, N., Weissman, D., and Whitehead, K.A. (2021). mRNA vaccines for infectious diseases: principles, delivery and clinical translation. Nat. Rev. Drug Discov. *20*, 817–838. https://doi.org/10.1038/s41573-021-00283-5.
5. Goyal, F., Chattopadhyay, A., Navik, U., Jain, A., Reddy, P.H., Bhatti, G.K., and Bhatti, J.S. (2023). Advancing Cancer Immunotherapy: The Potential of mRNA Vaccines As a Promising Therapeutic Approach. Adv. Ther. *7*, 2300255. https://doi.org/10.1002/adtp.202300255.
6. Zhu, Y., Zhu, L., Wang, X., and Jin, H. (2022). RNA-based therapeutics: an overview and prospectus. Cell Death Dis. *13*, 644. https://doi.org/10.1038/s41419-022-05075-2.
7. Kauffman, K.J., Webber, M.J., and Anderson, D.G. (2016). Materials for non-viral intracellular delivery of messenger RNA therapeutics. J. Control. Release *240*, 227–234. https://doi.org/10.1016/j.jconrel.2015.12.032.
8. Schoenmaker, L., Witzigmann, D., Kulkarni, J.A., Verbeke, R., Kersten, G., Jiskoot, W., and Crommelin, D.J.A. (2021). mRNA-lipid nanoparticle COVID-19 vaccines: Structure and stability. Int. J. Pharm. *601*, 120586. https://doi.org/10.1016/j.ijpharm.2021.120586.
9. Crommelin, D.J.A., Anchordoquy, T.J., Volkin, D.B., Jiskoot, W., and Mastrobattista, E. (2021). Addressing the Cold Reality of mRNA Vaccine Stability. J. Pharm. Sci. *110*, 997–1001. https://doi.org/10.1016/j.xphs.2020.12.006.
10. Muramatsu, H., Lam, K., Bajusz, C., Laczkó, D., Karikó, K., Schreiner, P., Martin, A., Lutwyche, P., Heyes, J., and Pardi, N. (2022). Lyophilization provides long-term stability for a lipid nanoparticle-formulated, nucleoside-modified mRNA vaccine. Mol. Ther. *30*, 1941–1951. https://doi.org/10.1016/j.ymthe.2022.02.001.
11. Zimmermann, C.M., Deßloch, L., Jürgens, D.C., Luciani, P., and Merkel, O.M. (2023). Evaluation of the effects of storage conditions on spray-dried siRNA-LNPs before and after subsequent drying. Eur. J. Pharm. Biopharm. *193*, 218–226. https://doi.org/10.1016/j.ejpb.2023.11.007.
12. Zimmermann, C.M., Baldassi, D., Chan, K., Adams, N.B.P., Neumann, A., Porras-Gonzalez, D.L., Wei, X., Kneidinger, N., Stoleriu, M.G., Burgstaller, G., et al. (2022). Spray drying siRNA-lipid nanoparticles for dry powder pulmonary delivery. J. Control. Release *351*, 137–150. https://doi.org/10.1016/j.jconrel.2022.09.021.
13. Gerhardt, A., Voigt, E., Archer, M., Reed, S., Larson, E., Van Hoeven, N., Kramer, R., Fox, C., and Casper, C. (2022). A flexible, thermostable nanostructured lipid carrier platform for RNA vaccine delivery. Mol. Ther. Methods Clin. Dev. *25*, 205–214. https://doi.org/10.1016/j.omtm.2022.03.009.
14. Nele, V., Campani, V., and De Rosa, G. (2024). Liposomes as DNA, mRNA and oligonucleotide delivery vectors. In Liposomes in Drug Delivery, S.G. Antimisiaris, ed. (Elsevier), pp. 303–328. https://doi.org/10.1016/B978-0-443-15491-1.00012-2.
15. Nele, V., Campani, V., Alia Moosavian, S., and De Rosa, G. (2024). Lipid nanoparticles for RNA delivery: Self-assembling vs driven-assembling strategies. Adv. Drug Deliv. Rev. *208*, 115291. https://doi.org/10.1016/j.addr.2024.115291.
16. Campani, V., Giarra, S., and De Rosa, G. (2018). Lipid-based core-shell nanoparticles: Evolution and potentialities in drug delivery. OpenNano *3*, 5–17. https://doi.org/10.1016/j.onano.2017.12.001.
17. Cai, A., Zhu, Y., and Qi, C. (2020). Biodegradable Inorganic Nanostructured Biomaterials for Drug Delivery. Adv. Mater. Interfaces *7*, 2000819. https://doi.org/10.1002/admi.202000819.
18. Salzano, G., Marra, M., Porru, M., Zappavigna, S., Abbruzzese, A., La Rotonda, M.I., Leonetti, C., Caraglia, M., and De Rosa, G. (2011). Self-assembly nanoparticles for the delivery of bisphosphonates into tumors. Int. J. Pharm. *403*, 292–297. https://doi.org/10.1016/j.ijpharm.2010.10.046.
19. Marra, M., Salzano, G., Leonetti, C., Porru, M., Franco, R., Zappavigna, S., Liguori, G., Botti, G., Chieffi, P., Lamberti, M., et al. (2012). New self-assembly nanoparticles and stealth liposomes for the delivery of zoledronic acid: a comparative study. Biotechnol. Adv. *30*, 302–309. https://doi.org/10.1016/j.biotechadv.2011.06.018.

20. Porru, M., Zappavigna, S., Salzano, G., Luce, A., Stoppacciaro, A., Balestrieri, M.L., Artuso, S., Lusa, S., De Rosa, G., Leonetti, C., and Caraglia, M. (2014). Medical treatment of orthotopic glioblastoma with transferrin-conjugated nanoparticles encapsulating zoledronic acid. Oncotarget *5*, 10446–10459. https://doi.org/10.18632/oncotarget.2182.

21. Campani, V., Zappavigna, S., Scotti, L., Abate, M., Porru, M., Leonetti, C., Caraglia, M., and De Rosa, G. (2020). Hybrid lipid self-assembling nanoparticles for brain delivery of microRNA. Int. J. Pharm. *588*, 119693. https://doi.org/10.1016/j.ijpharm.2020.119693.

22. Delle Donne, R., Iannucci, R., Rinaldi, L., Roberto, L., Oliva, M.A., Senatore, E., Borzacchiello, D., Lignitto, L., Giurato, G., Rizzo, F., et al. (2022). Targeted inhibition of ubiquitin signaling reverses metabolic reprogramming and suppresses glioblastoma growth. Commun. Biol. *5*, 780. https://doi.org/10.1038/s42003-022-03639-8.

23. Vangasseri, D.P., Cui, Z., Chen, W., Hokey, D.A., Falo, L.D., and Huang, L. (2006). Immunostimulation of dendritic cells by cationic liposomes. Mol. Membr. Biol. *23*, 385–395. https://doi.org/10.1080/09687860600790537.

24. Yan, W., Chen, W., and Huang, L. (2007). Mechanism of adjuvant activity of cationic liposome: Phosphorylation of a MAP kinase, ERK and induction of chemokines. Mol. Immunol. *44*, 3672–3681. https://doi.org/10.1016/j.molimm.2007.04.009.

25. Ristori, S., Grillo, I., Lusa, S., Thamm, J., Valentino, G., Campani, V., Caraglia, M., Steiniger, F., Luciani, P., and De Rosa, G. (2018). Structural Characterization of Self-Assembling Hybrid Nanoparticles for Bisphosphonate Delivery in Tumors. Mol. Pharm. *15*, 1258–1265. https://doi.org/10.1021/acs.molpharmaceut.7b01085.

26. Martinez, D.S.T., Paula, A.J., Fonseca, L.C., Luna, L.A.V., Silveira, C.P., Durán, N., and Alves, O.L. (2015). Monitoring the Hemolytic Effect of Mesoporous Silica Nanoparticles after Human Blood Protein Corona Formation. Eur. J. Inorg. Chem. *2015*, 4595–4602. https://doi.org/10.1002/ejic.201500573.

27. Blanco, E., Shen, H., and Ferrari, M. (2015). Principles of nanoparticle design for overcoming biological barriers to drug delivery. Nat. Biotechnol. *33*, 941–951. https://doi.org/10.1038/nbt.3330.

28. Francia, V., Schiffelers, R.M., Cullis, P.R., and Witzigmann, D. (2020). The Biomolecular Corona of Lipid Nanoparticles for Gene Therapy. Bioconjug. Chem. *31*, 2046–2059. https://doi.org/10.1021/acs.bioconjchem.0c00366.

29. Gunawan, C., Lim, M., Marquis, C.P., and Amal, R. (2014). Nanoparticle–protein corona complexes govern the biological fates and functions of nanoparticles. J. Mater. Chem. B *2*, 2060–2083. https://doi.org/10.1039/c3tb21526a.

30. Zaias, J., Mineau, M., Cray, C., Yoon, D., and Altman, N.H. (2009). Reference values for serum proteins of common laboratory rodent strains. J. Am. Assoc. Lab. Anim. Sci. *48*, 387–390.

31. Dominiczak, M.H., and Caslake, M.J. (2011). Apolipoproteins: metabolic role and clinical biochemistry applications. Ann. Clin. Biochem. *48*, 498–515. https://doi.org/10.1258/acb.2011.011111.

32. Passariello, M., Gentile, C., Ferrucci, V., Sasso, E., Vetrei, C., Fusco, G., Viscardi, M., Brandi, S., Cerino, P., Zambrano, N., et al. (2021). Novel human neutralizing mAbs specific for Spike-RBD of SARS-CoV-2. Sci. Rep. *11*, 11046. https://doi.org/10.1038/s41598-021-90348-7.

33. Prompetchara, E., Ketloy, C., Alameh, M.-G., Tharakhet, K., Kaewpang, P., Yostrerat, N., Pitakpolrat, P., Buranapraditkun, S., Manopwisedjaroen, S., Thitithanyanont, A., et al. (2023). Immunogenicity and protective efficacy of SARS-CoV-2 mRNA vaccine encoding secreted non-stabilized spike in female mice. Nat. Commun. *14*, 2309. https://doi.org/10.1038/s41467-023-37795-0.

34. Tanaka, H., Sato, Y., Nakabayashi, T., Tanaka, A., Nishio, K., Matsumoto, C., Matsumaru, A., Yamakawa, T., Ishizaki, K., Ueda, K., et al. (2025). A Post-Encapsulation Method for the Preparation of mRNA-LNPs via the Nucleic Acid-Bridged Fusion of mRNA-Free LNPs. Nano Lett. *25*, 6445–6453. https://doi.org/10.1021/acs.nanolett.4c06643.

35. Jones, K.L., Drane, D., and Gowans, E.J. (2007). Long-Term Storage of DNA-Free RNA for use in Vaccine Studies. Biotechniques *43*, 675–681. https://doi.org/10.2144/000112593.

36. Alam, S.B., Wang, F., Qian, H., and Kulka, M. (2023). Apolipoprotein C3 facilitates internalization of cationic lipid nanoparticles into bone marrow-derived mouse mast cells. Sci. Rep. *13*, 431. https://doi.org/10.1038/s41598-022-25737-7.

37. Dilliard, S.A., Sun, Y., Brown, M.O., Sung, Y.-C., Chatterjee, S., Farbiak, L., Vaidya, A., Lian, X., Wang, X., Lemoff, A., and Siegwart, D.J. (2023). The interplay of quaternary ammonium lipid structure and protein corona on lung-specific mRNA delivery by selective organ targeting (SORT) nanoparticles. J. Control. Release *361*, 361–372. https://doi.org/10.1016/j.jconrel.2023.07.058.

38. Haab, B.B., Geierstanger, B.H., Michailidis, G., Vitzthum, F., Forrester, S., Okon, R., Saviranta, P., Brinker, A., Sorette, M., Perlee, L., et al. (2005). Immunoassay and antibody microarray analysis of the HUPO Plasma Proteome Project reference specimens: Systematic variation between sample types and calibration of mass spectrometry data. Proteomics *5*, 3278–3291. https://doi.org/10.1002/pmic.200401276.

39. Dilliard, S.A., Cheng, Q., and Siegwart, D.J. (2021). On the mechanism of tissue-specific mRNA delivery by selective organ targeting nanoparticles. Proc. Natl. Acad. Sci. USA *118*, e2109256118. https://doi.org/10.1073/pnas.2109256118.

40. Rusciano, G., Sasso, E., Capaccio, A., Zambrano, N., and Sasso, A. (2019). Revealing membrane alteration in cells overexpressing CA IX and EGFR by Surface-Enhanced Raman Scattering. Sci. Rep. *9*, 1832. https://doi.org/10.1038/s41598-018-37997-3.

41. Sasso, E., Froechlich, G., Cotugno, G., D'Alise, A.M., Gentile, C., Bignone, V., De Lucia, M., Petrovic, B., Campadelli-Fiume, G., Scarselli, E., et al. (2020). Replicative conditioning of Herpes simplex type 1 virus by Survivin promoter, combined to ERBB2 retargeting, improves tumour cell-restricted oncolysis. Sci. Rep. *10*, 4307. https://doi.org/10.1038/s41598-020-61275-w.

42. D'Alise, A.M., Nocchi, L., Garzia, I., Seclì, L., Infante, L., Troise, F., Cotugno, G., Allocca, S., Romano, G., Lahm, A., et al. (2023). Adenovirus Encoded Adjuvant (AdEnA) anti-CTLA-4, a novel strategy to improve Adenovirus based vaccines against infectious diseases and cancer. Front. Immunol. *14*, 1156714. https://doi.org/10.3389/fimmu.2023.1156714.

43. Troise, F., Leoni, G., Sasso, E., Del Sorbo, M., Esposito, M., Romano, G., Allocca, S., Froechlich, G., Cotugno, G., Capone, S., et al. (2024). Prime and pull of T cell responses against cancer-exogenous antigens is effective against CPI-resistant tumors. Mol. Ther. Oncol. *32*, 200760. https://doi.org/10.1016/j.omton.2024.200760.

44. Lee, G.Y., Li, A.A., Moon, I., Katritsis, D., Pantos, Y., Stingo, F., Fabbrico, D., Molinaro, R., Taraballi, F., Tao, W., and Corbo, C. (2024). Protein Corona Sensor Array Nanosystem for Detection of Coronary Artery Disease. Small *20*, e2306168. https://doi.org/10.1002/smll.202306168.

45. Corbo, C., Li, A.A., Poustchi, H., Lee, G.Y., Stacks, S., Molinaro, R., Ma, P., Platt, T., Behzadi, S., Langer, R., et al. (2021). Analysis of the Human Plasma Proteome Using Multi-Nanoparticle Protein Corona for Detection of Alzheimer's Disease. Adv. Healthc. Mater. *10*, e2000948. https://doi.org/10.1002/adhm.202000948.

46. Contessotto, P., Orbanić, D., Da Costa, M., Jin, C., Owens, P., Chantepie, S., Chinello, C., Newell, J., Magni, F., Papy-Garcia, D., et al. (2021). Elastin-like recombinamers-based hydrogel modulates post-ischemic remodeling in a non-transmural myocardial infarction in sheep. Sci. Transl. Med. *13*, eaaz5380. https://doi.org/10.1126/scitranslmed.aaz5380.

47. Previtali, P., Pagani, L., Risca, G., Capitoli, G., Bossi, E., Oliveira, G., Piga, I., Radice, A., Trezzi, B., Sinico, R.A., et al. (2023). Towards the Definition of the Molecular Hallmarks of Idiopathic Membranous Nephropathy in Serum Proteome: A DIA-PASEF Approach. Int. J. Mol. Sci. *24*, 11756. https://doi.org/10.3390/ijms241411756.